THE JOURNAL OF PHYSICAL CHEMISTRY C

Article

pubs.acs.org/JPCC

Perovskite—Cavity Complex: the Modulated Optical Characteristics of Organometallic Halide Perovskite $CH_3NH_3PbI_xCl_{3-x}$ Doped in Length Tunable Optical Microcavities

Zhen-Yu Zhang,[†] Hai-Yu Wang,*[,†] Kai-Jiao Li,[‡] Ming Xu,[†] Hai Wang,[†] Bing-Rong Gao,[†] Qi-Dai Chen,[†] and Hong-Bo Sun*[,†]

[†]State Key Laboratory on Integrated Optoelectronics, College of Electronic Science and Engineering, and [‡]College of Physics, Jilin University, 2699 Qianjin Street, Changchun 130012, China

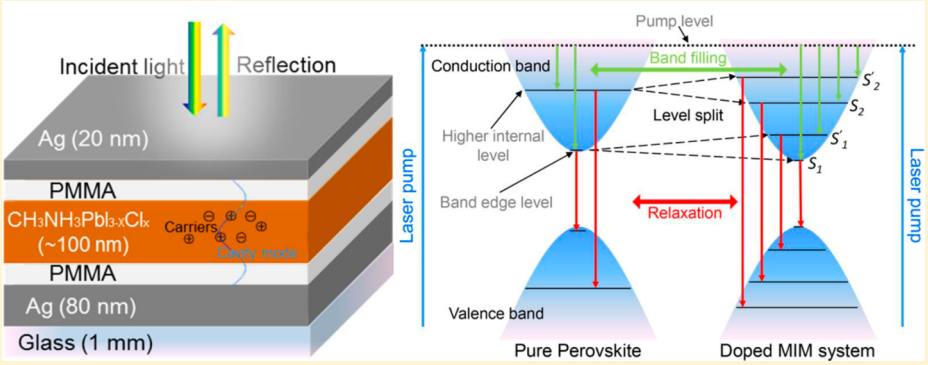

ABSTRACT: When organometallic halide perovskite semiconductors with continuous transition band were placed into an optical microcavity, interaction/modulation effect between confined photonic mode supported by cavity and free charge carriers mode triggered in perovskite occurred. In this metal−insulator−metal (MIM) microcavity, given the broad absorption region of perovskite $CH_3NH_3PbI_xCl_{3-x}$, the cavity resonant energy can be selectively designed to modulate the photophysical characteristics of perovskite charge carriers at different levels. Another advantage of using perovskite is that its band filling effect (charge carrier's accumulation process) and relaxation process could last for few and hundreds picoseconds respectively, allowing us to accurately examine the time-resolved couple modulating effect by microcavities. Steady-state and transient absorption (TA) spectra were carried out to experimentally confirm the modulation effect of microcavity on optical characteristics of perovskite free charge carriers. It is found that created binate new states around cavity-perovskite resonance emerged at different perovskite levels are mutually independent. Interestingly, the band filling process of these new states is found not affected while their fluence-dependent relaxation process is accelerated by microcavities. The results in our work show that we can selectively manipulate the optical characteristics (absorption and charge carriers lifetimes) of perovskite by length tunable optical microcavities. Our efforts may propose an interesting modulating system and trigger potential optical application based on perovskite−light complex.

INTRODUCTION

Semiconductor doped metal−insulator−metal (MIM) microcavities offer an ideal platform to study the coupling effect between confined electromagnetic and matter at nanoscale.[1−7] Within a very small confined volume in a cavity, there will be a reversible energy exchange between photon and matter, this formed quasiparticle is so-called cavity polaritons.[6] Interest in this area was first theoretically analyzed by E. T. Jaynes and F. W. Cummings in 1963,[8] henceforth, their proposed Jaynes—Cummings model (so-called J-C mode) was commonly used to describe the coupling between a single atom and the quantized optical field.[9−13] Fortunately, due to the development of semiclassical cavity quantum electrodynamics (cQED), the J-C mode can also be applied to a semiclassical microcavity in the real world.[1] In 1997, strong interaction between a confined photonic mode supported by a microcavity and a two-level atom was first observed by Weisbuch group.[14] These theory and experiment at early time demonstrated that aims to realize energy exchange in MIM microcavities, the cavity resonance should be first tuned to the same value with atom absorption transition. More importantly, the coupling strength between light and matter should also be designed far exceeded the losses intensity of cavity radiation and atom spontaneous emission.[9−11,14,15] The generated states exhibit absolute new optical properties and this phenomenon renders MIM microcavity as an ideal test bed for the coupling effect in cavity−matter complex system. In the past decades, a series of coupling phenomenon have been demonstrated in microcavities

Received: April 22, 2016
Revised: May 24, 2016
Published: June 1, 2016

DOI: 10.1021/acs.jpcc.6b04072
J. Phys. Chem. C 2016, 120, 13295−13302

containing J-aggregates,[11,16−20] nanostructure,[1−3,21−23] and molecular crystals polymers.[24−26] Recently, it also shows that the MIM-analogous nanostructures potentially provide a means to reduce emission thresholds and this effect makes such MIM systems more attractive for optical amplifiers and low threshold lasers applications.[27−30]

In the MIM coupling system, the optical characteristics of matter are changed by microcavities through a coupling effect; from another aspect, this phenomenon can be considered as the modulation effect of microcavity resonance on the matter level transition. The past few years have witnessed the increasing breakthroughs in the theoretical and experimental studied on MIM analogous cavity−matter complex system because of the rapid development of fabrication and characterization for micro/nano-objects.[31−35] Through these great efforts, people have found an effective way of modulating the energy redistribution and relaxation process in these system.[21,33−35] More and more time-resolved studies[27,31−33,36] have been performed on the photophysics in cavity−matter complex system, especially on the new states emerged around cavity−matter resonance. A recent review has concluded a nice summary and provided a relative comprehensive understanding on these issues from classical, semiclassical, and fully quantum aspects.[37] In the case of modulation effect of microcavity, although many effects have been reported, some fundamental photophysical questions still remained unresolved. Such as whether new states (modulation effects) occurred when the excite species of the embedded matter was free charge carriers rather than conventional exciton? How to realize the modulation when the embedded matter possesses continuous ultrabroad transition levels rather than typical two-level system? Moreover, considering the relative slower charge carrier's accumulation and recombination rates in perovskite, we also want to know how the dynamics of perovskite are influenced by microcavities?

As far as we are aware, this work differs from previously MIM microcavities as the embedded perovskite $CH_3NH_3PbI_xCl_{3-x}$ exhibiting the ultrabroad continuous absorption level transition ranging from 400 to 800 nm and its excited species is mainly dominated by free charge carriers.[38] We argue that modulation effect will play a key role in determining the optical properties of the embedded perovskite layers. In the present work, performing reflective steady-state and time-resolved transient absorption (TA) spectroscopy measurements, we show the existence of new states created around cavity-matter resonance and these binate states created at different perovskite level are mutual independent. We also modeled the dynamics of new states, and the results show that the band filling processes are hardly affected while the relaxation processes are accelerated by microcavities. These new states are half-cavity and half-carriers, causing the resultant relaxation processes are not only faster than bare perovskite films, but also fluences-dependent. Details will be discussed in the following.

EXPERIMENTAL SECTION AND THEORY

The structure of studied perovskite—cavity complex MIM system is shown schematically in Figure 1a. The MIM microcavity contains a ∼100 nm thick layer organometal halide $CH_3NH_3PbI_xCl_{3-x}$ perovskite film caught in the interlayer of double-deck poly(methyl methacrylate) (PMMA), which was sandwiched between two metallic sliver mirrors. This microstructure is started from 80 nm thick silver mirror, which was thermally evaporated onto a 1 mm thick glass substrate.

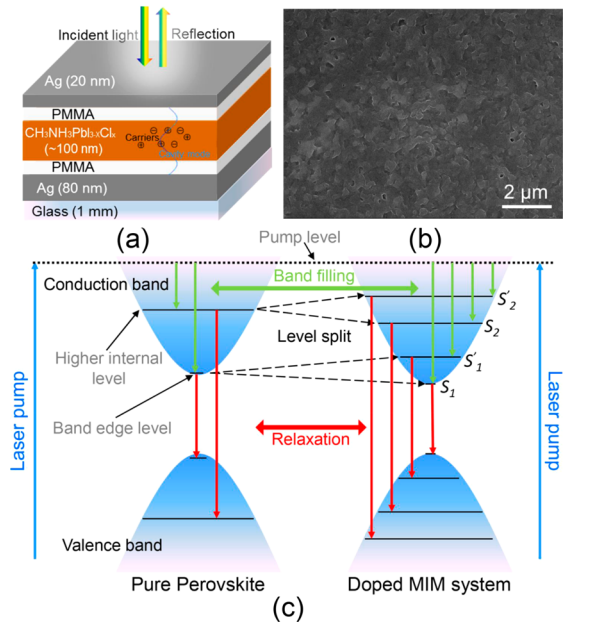

Figure 1. (a) Schematic of the studied MIM microcavity containing a layer of $CH_3NH_3PbI_xCl_{3-x}$ perovskite. (b) Top-view scanning electron microscope (SEM) micrograph of perovskite layer, the bar is 2 μm. (c) The typical Jablonski diagrams of bare perovskite phase (left) and doped MIM system (right).

Subsequently, a layer of PMMA is spin-casted onto the sliver film to avoid the contact between Ag films and $CH_3NH_3PbI_xCl_{3-x}$ layers. Then a solution of the perovskite precursor in a *N*,*N*-dimethylformamide (DMF) solution (wt ∼20%) mixed at 3:1 ($CH_3NH_3I/PbCl_2$) quality ratio was spin-cast (3000 rpm) onto the PMMA layer and then the films was crystallized to perovskite grains films through thermal annealing at ∼80 °C for 100 min in a nitrogen filled glovebox. Another layer of PMMA separated the $CH_3NH_3PbI_xCl_{3-x}$ from the top sliver mirror. At last, a 20 nm thick semitransparent silver mirror is thermal evaporated onto the top of this MIM microcavity. Microcavities are carefully designed to have the same resonance with perovskite charge carriers at different levels. Theoretically, the *N*th microcavities resonant wavelength can be defined[1,2] as $\lambda_N = 2n_d(L + \delta)/N$, where n_d is the effect refractive index, the L denotes the thickness of the coated spacer (perovskite and PMMA layers) between two sliver mirrors, and the δ is attributed to the reflection phase (∼100 nm). Experimentally, the expression told us that we can easily controlling the microcavity resonant by changing the thickness of spacer and we selectively prepared three microcavities with different L. Their effective optical path length is designed as ∼760, ∼1100, and ∼2100 nm, in short, these three MIM systems are named as cavity A, B, and C, respectively. The *Q*-factor (defined as the cavity half-height line-width divided by its resonant wavelength ω_c) of the cavity is calculated as about 15, indicating confined-photon lifetime $\tau_c = Q/\omega_c$ at ∼30 fs. Figure 1b shows the top-view scanning electron microscope (SEM) image of embedded perovskite layers, the bar is 2 μm. The crystallized perovskite grains are found fully covered the PMMA layer with sizes ranging from 200 to 250 nm. Figure 1c illustrates the typical Jablonski diagram of bare perovskite phase and doped MIM system. The left part of the diagram shows that the perovskite exhibiting continuous level transition, here, we mainly focused on the band edge level (∼745 nm) and band

DOI: 10.1021/acs.jpcc.6b04072
J. Phys. Chem. C 2016, 120, 13295−13302

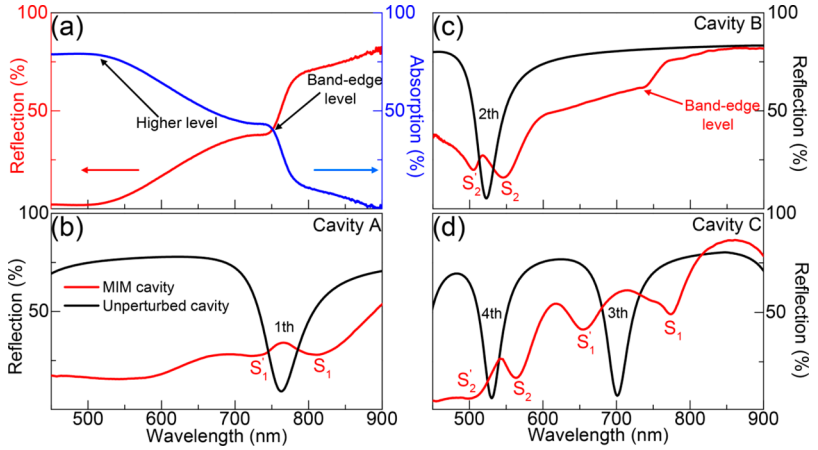

Figure 2. (a) Reflection (red line) and absorption (blue line) spectrum obtained for bare perovskite films thermally crystallized on a sliver mirror separated by a layer of PMMA and glass substrates, respectively. (b–d) Plots of the measured optical reflect spectra (red line) and simulated unperturbed cavity resonance (black line) for MIM microcavities A, B, and C, respectively. Their effective optical path length is designed as ∼760, ∼1100, and ∼2100 nm.

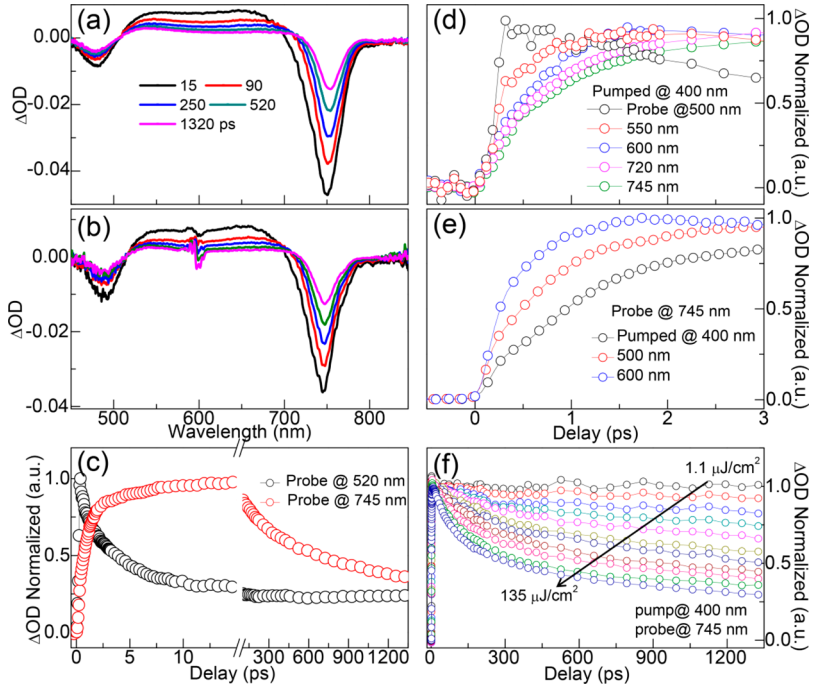

Figure 3. (a, b) Time-resolved transient absorption spectra of bare $CH_3NH_3PbI_xCl_{3-x}$ perovskite layer at different probe delay times pumped with 400 and 600 nm, respectively. (c) Normalized bleaching kinetics of band internal level (520 nm) and band-edge level (745 nm) of perovskite carriers after excitation at 400 nm. (d) Normalized signals build-up process (pumped with 400 nm) at different probe wavelengths ranging from 500 to 745 nm, the band filling process becomes slower with increasing carriers energy. (e) band-edge probe (745 nm) at different excitation wavelengths, analogous to (d), the signal build-up process becomes more slower with increasing energy difference between pump and probe wavelengths. (f) Transient band-edge bleaching kinetics at 745 nm after 400 nm excitation with a series of pump fluences ranging from 1.1 to 135 $\mu J/cm^2$. Higher carriers' density results into an increasing relaxation rates at band-edge.

internal level (∼520 nm). Following pump excitation, charge carriers in condensed phases would first jump from pump level to band edge level and band internal level, respectively (so-called band filling process), and then slowly relax back to valence band. In perovskite-doped MIM system shown in the right part, according to J-C mode and semiclassical cQED,[1] original perovskite levels are split into binate new states. In the MIM system, the new states created around band edge is named as S'_1 and S_1, created around band internal level is named as S'_2 and S_2. Under the manipulation of microcavities, the triggered charge carriers in condensed phases would first jump from pump level to new state levels and then slowly relax back to valence band. In order to examine the manipulation effect of microcavities on the perovskite charge carriers, we carried out reflective steady and transient spectrum experiments. Steady-state reflection spectroscopy was obtained by a Shimadzu UV-2550 spectrophotometer and time-resolved reflective TA spectroscopy was carried out by a femtosecond (fs) pump–probe system. Briefly, our fs-TA setup is mainly composed of by a Spitfire Pro System (Spectra-Physics) that outputs 800 nm lasers (∼100 fs) with pulse energy about 1.1 mJ. The 800 nm laser with repetition rate of 250 Hz is split to

DOI: 10.1021/acs.jpcc.6b04072
J. Phys. Chem. C 2016, 120, 13295–13302

two parts, sending one part through frequency doubling β-barium borate (BBO) crystal to produce 400 nm lasers. This beam is modulated by an optical chopper (Newport Model 75160) with a frequency of 125 Hz as the pump beam to excite the sample after going through a delay line (Newport M-ILS250CC). The other part is penetrated into a sapphire crystal to generate continuous white light as the probe beam ranging from 450 to 800 nm. The probe beam which reflected by sample was collected by a highly sensitive spectrometer (AvaSpec-2048 × 14). The measured data are disposed by a chirp program.

RESULTS AND DISCUSSION

Steady-State Optical Properties. We check out the optical reflective spectra for these microcavities A, B, and C, whose effective path length is ∼760, ∼1100, and ∼2100 nm, respectively. Bare perovskite films coated on glass and on 80 nm sliver mirror separated by a layer of PMMA are as reference, their absorption (blue line) and reflection (red line) spectra are shown in Figure 2a. Figure 2b–d plotted the measured optical reflective spectra (red line) and simulated unperturbed cavity resonance spectra (blue line) of MIM microcavities A, B, and C, respectively. It can be learned from Figure 2a that the perovskite differs from other exciton materials[11,16−20] as it exhibits continuous absorption transition throughout the entire visible spectrum. Here, we mainly focused on the band edge level around 750 nm and band internal level around 520 nm. In order to realize the energy exchange between cavity resonance and perovskite charge carriers at different perovskite levels, the total effective optical paths of microcavities A, B, and C are, respectively, designed as 760, 1100, and 2100 nm. In cavity A (Figure 2b), 1st mode of 760 nm is resonated with band edge level around 745 nm, generating a pair of new states with S'_1 at 733 nm and S_1 at 820 nm. The level splitting intensity is calculated about 190 meV. Far from the microcavity resonance, the perovskite band internal level around 520 nm can also be readily observed. In cavity B (Figure 2c), interaction occurred between 2nd mode of 520 nm and band internal level, showing S'_2 at 500 nm and S_2 at 550 nm with level split intensity at 225 meV. Similar to cavity A, without the disturbance of cavity resonance, it is also clear to observe the typical perovskite band edge absorption transition around 745 nm. In cavity C (Figure 2d), 3rd (701 nm) and 4th (526 nm) cavity resonances are shown to be simultaneously interacted with the closer band edge and band internal levels, respectively. The interaction around band edge shows the split intensity of 248 meV with S'_1 at 658 nm and S_1 at 768 nm, around band internal level shows the split intensity of 235 meV with S'_2 at 512 nm and S_2 at 567 nm. These new dips in steady-state reflection spectra are indicative of the existence of new states in these perovskite—cavity complex system. Nevertheless, we still cannot get the nature of these new states, for a better understanding, difference TA spectroscopy measurements are carried out.

TA Measurement on Bare $CH_3NH_3PbI_xCl_{3-x}$ Films. First, we need get a relative comprehensive understanding on bare $CH_3NH_3PbI_xCl_{3-x}$ films. Figure 3a and b show the TA spectra of bare perovskite films pumped with 400 and 600 nm, respectively. The spectra show two obvious ground state bleaching (GSB) signals at 750 nm (it is equals to the band edge level) and 485 nm (it had been previously demonstrated caused by the crystal decomposition[39]), as well as the broad excited state absorption (ESA) signals ranging from 500 to 700 nm. Figure 3c shows the kinetics curves of band edge level around 745 nm (red circle) and band internal level around 520 nm (black circle) pumped under 400 nm. The slow transient bleaching build-up in ∼10 ps of 745 nm is indicative of the charge carrier accumulation based on the band filling effect. While the dynamic of 520 nm shows a very fast bleaching build-up, which is close to the laser pulse duration. Moreover, the decay curve of 520 nm shows faster relaxation rates than that of 745 nm. The difference can be attributed that the excited species at shorter wavelengths is more exciton-like, causing the abrupt rising edge during buildup and rapid decay during relaxation. As shown in Figure 3d, with pump under 400 nm, the excited species becomes more exciton-like when probe wavelengths gradually blue-shift from 745 to 500 nm, caused the resultant accelerating signal build-up process. Figure 3e shows the signal build-up process of band edge under different pump energy. Due to increasing excess energy when pumped energy increased from 600 to 400 nm, it reads that the band filling process becomes slower.[40] Figure 3f shows the decay dynamics of band edge at 745 nm under a range of pump fluences between 1.1 and 135 $\mu J/cm^2$. In the presence of free charge carriers at 745 nm, the carriers relax dynamics will show strong pump-intensity dependence: the kinetic recombination rates become faster with increasing pump intensities. The arrow indicates the direction of increasing pump fluences.

TA Measurement on MIM System under Nonresonant Excitation. We performed time-resolved reflective difference TA measurements on perovskite doped MIM microcavities A, B and C. These TA spectra are taken following nonresonant pump excitation at 400 nm with fluence at 85 $\mu J/cm^2$. These spectra show photoinduced bleach recovery processes as a function of delay time. Figure 4a, b, and c, respectively, shows the TA spectra of perovskite—cavity complex MIM microcavities A, B, and C. As respected, each spectrogram shows that the binate new GSB signals emerged around perovskite-cavity

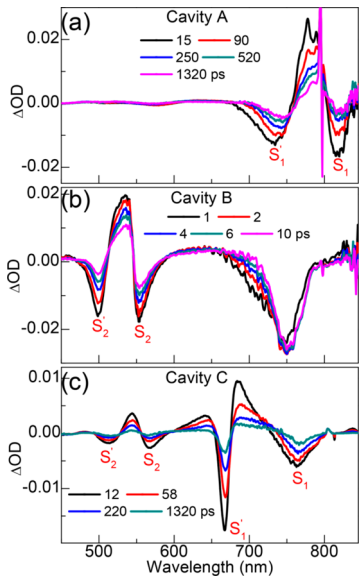

Figure 4. (a, b, and c) Evolution of transient differential absorbance spectra after excitation under 400 nm (85 $\mu J/cm^2$) for MIM microcavities A, B, and C, respectively. As respect, new binate GSB signals emerged in these spectrograms show the same wavelengths with the steady-states results in Figure 2. The positive signals are mainly caused by the absorption of the populated states to higher excited states.

DOI: 10.1021/acs.jpcc.6b04072
J. Phys. Chem. C 2016, 120, 13295−13302

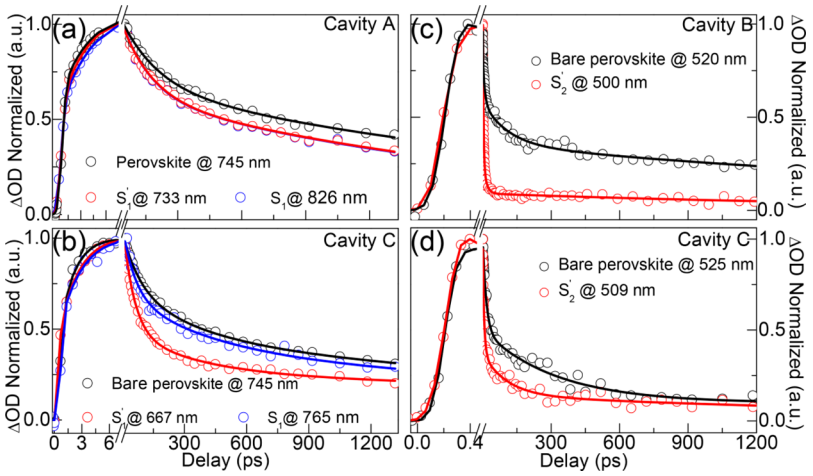

Figure 5. These dynamics curves pumped under 400 nm are split into two parts with the signal buildup representing band filling process and signal decay denoting relaxation process. The bare perovskite (black dots and lines) is as the reference. (a, b) Dynamics of S'_1 and S_1, respectively, created around band-edge level (~745 nm) in cavities A and C. (c, d) Dynamics of S'_2 created around band internal level (520 nm) in cavities B and C, respectively.

resonance and the wavelengths are consistent with the steady-states results from Figure 2. In Figure 4a (cavity A), as respect, the TA spectra show two negative distinctive bleaching signatures at 733 (S'_1) and 820 (S_1) nm as well as the big positive ESA signals centered at 775 nm. The negative signals indicate the existence of new states and the positive signals is caused by the absorption of the populated states to higher excited states.[32] Moreover, the band internal level transition of bare perovskite which away from cavity resonance has been shield for the sliver films, causing the resultant intensity of ΔOD signals bellowing 660 nm is almost zero. In Figure 4b (cavity B), expect the S'_2 (500 nm) and S_2 (550 nm), the spectra also shows a strong positive ESA signals at 525 nm. Analogous to cavity A, the positive ESA signals can be partly associated with absorption from 525 nm toward higher states and partly due to the intrinsic ESA of bare perovskite (shown in Figure 3a). Interestingly, though the band edge is far away from cavity resonance, one still can read the corresponding signal due to its strong TA signals intensity. In Figure 4c (cavity C), the band-edge and band internal level of perovskite are modulated by microcavity simultaneously. These two binate new GSB signals show the same wavelengths compared with steady-state results. Analogous to cavities A and B, the spectra also show the positive signals at 543 and 685 nm. The positive signal at 640 nm is not influenced by cavity resonance, so it can only be attributed to the intrinsic ESA signals of bare perovskite. These difference TA results are of direct proof for modulation effects of microcavities on the embedded perovskite layer in the perovskite−cavity complex system.

Band Filling and Relaxation Process Pumped under 400 nm. Our time-resolved femtosecond pump−probe technology allowed us to investigate how the microcavities modulate the perovskite charge carriers' transient characteristics by checking out the band filling and recombine relaxation process of new states. Figure 5a,c illustrates the integral kinetics of these new states emerged around band edge level (in cavity A) and band internal level (in cavity B), respectively. Figure 5b,d shows the integral kinetics of new states, which are simultaneously created around band edge and band internal level in cavity C respectively. These kinetics curves are broken into two parts as a function of delay time. The early buildup dynamics show the band filling processes and the latter decay dynamics show carriers relaxation process. We fitted these kinetics curves (lines) as a combination of signal buildup and decay components. In Figure 5a (cavity A), band filling processes of new states are show almost all the same with that of bare perovskite phase, the fitted buildup lifetime are 4.815 ± 0.02 ps for S'_1, 4.912 ± 0.02 ps for S_1, and 4.995 ± 0.02 ps for perovskite band edge transition. While the relaxation processes of S'_1 and S_1 are accelerated by microcavity. Due to symmetrical distribution, the new states show the same relaxation line-style with fitted lifetime at 1250 ± 6 ps, faster than that of bare perovskite films fitted at 1570 ± 8 ps. In cavity A, the microcavity resonance energy (770 nm) is much lower than the charge carriers with excess energy, which jumped from 400 nm, so the band filling process can be hardly influenced by cavity resonance energy. While during the relaxation process, the charge carries of new states have the equivalent energy with cavity resonance and the resultant modulation effect occurred. In Figure 5c (cavity B), similar to cavity A, the early buildup dynamics are also not influenced by microcavities with the fitted buildup lifetimes are 0.385 ± 0.02 ps for S'_2 and 0.371 ± 0.02 ps for bare perovskite band internal transition at 520 nm. While the later decay dynamics shows that the lifetime of new state S'_2 (fitted at 150 ± 3 ps) is much faster than that of bare perovskite (fitted at 1150 ± 6 ps). From Figure 3, we have learned that the carriers' band filling and relaxation process is accelerated when probe wavelengths blue-shifted, as a result, the band filling and relaxation process of new states in cavity B is much faster than that of cavity A. From the couple modulating effect aspects, the factors of relaxation rates accelerated by cavity increased from 1.25 in cavity A to 7.6 in cavity B. This phenomenon can be attributed to that the excited species at higher states is more exciton-like, the possessed sufficient large energy triggers stronger manipulation effects. In Figure 5b and d (cavity C), we respectively fitted the kinetics of binate new states created around band edge level and band internal level. The dynamics of new states created around band edge in cavity C are similar to cavity A and new states created around band internal level in cavity C are similar to cavity B. This is a robust proof to verify these binate new states (or manipulation) at different levels are mutual independent. In

DOI: 10.1021/acs.jpcc.6b04072
J. Phys. Chem. C 2016, 120, 13295−13302

Figure 5b, the fitted signals buildup lifetimes/relaxation lifetimes are 4.545 ± 0.02/789 ± 5 ps for S'_1, 4.521 ± 0.02/1044 ± 6 ps for S_1, and 4.697 ± 0.02/1150 ± 6 ps for perovskite band edge transition. The different decay lifetimes of S'_1 and S_1 in cavity C can be contributed to the asymmetrical energy distribution: the S'_1 is closer to cavity mode, while S_1 is closer to perovskite band edge level, resulting in S'_1 is more cavity-like, while S_1 is more carriers-like. The kinetics of new states around band internal level in cavity C are illustrated in Figure 5d, as respect, similar to cavity B, the early buildup dynamics also shows changeless in microcavities. The fitted buildup lifetimes are 0.354 ± 0.02 ps for S'_2 and 0.361 ± 0.02 ps for perovskite band internal transition at 520 nm. The later decay dynamics shows that the lifetime of new state S'_2 (fitted at 221 ± 2 ps) is faster than that of bare perovskite at 525 nm (fitted at 303 ± 2 ps). It can be learned from Figure 4 that the band filling process from pump state to new states are almost unchanged while their relaxation processes are accelerated by cavity to different degrees. We also revealed the independent relationship of binate new states created at different levels.

Transient Characteristics of MIM System under Resonant Excitation. To get deeper understanding of the these perovskite−cavity complex MIM systems, we performed difference TA experiments under resonant excitation by 600 nm with fluence at 45 μJ/cm^2, which is selected to excite the states close to S'_1 created around band edge level or S_2 created around band internal level. According to the nature of cQED, the binate GSB signals of new states should be emerged simultaneously no matter which state is excited. Figure 6a, b, and c, respectively, show the difference TA spectra of MIM cavity A, B, and C pumped under 600 nm. As expected, these difference TA spectra show almost identical spectral shape compared with those from 400 nm excitation. These resonant pump−probe data fatherly also provide a robust proof of existent couple modulating effect in these perovskite-cavity complex MIM microcavities.

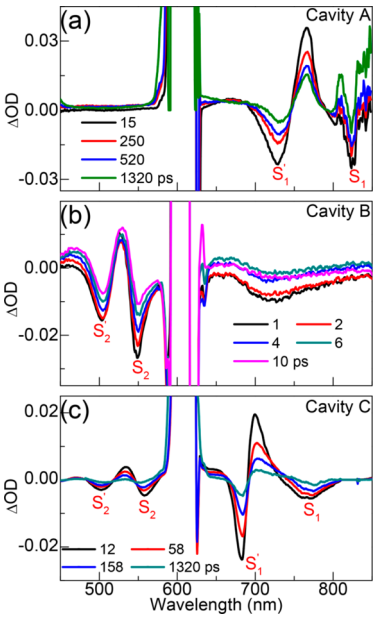

Figure 6. (a, b, and c) Evolution of transient differential absorbance spectra after excitation at 600 nm (45 μJ/cm^2) for MIM microcavities A, B, and C, respectivley. As respect, these spectrogram shows the almost the same line-shape with results pumped with 400 nm in Figure 4.

Representatively, Figure 7a and b, respectively, show the integral kinetics of S'_1 and S_1 created around the band edge in cavities A and C pumped under 600 nm. The kinetics shows almost the same behavior compared with the results pumped under 400 nm shown in Figure 5a,b. In Figure 7a (cavity A), the fitted signals buildup times/decay lifetimes are 2.865 ± 0.01/542 ± 4 ps for S'_1, 2.852 ± 0.01/556 ± 4 ps for S_1, and 2.843 ± 0.01/605 ± 5 ps for perovskite band edge transition. In Figure 7b (cavity C), the fitted buildup times/decay lifetimes are 2.866 ± 0.01/269 ± 3 ps for S'_1, 2.849 ± 0.01/465 ± 4 ps for S_1, and 2.845 ± 0.01/595 ± 5 ps for perovskite band edge transition. From Figure 3e, we have learned that due to the increasing excess energy when pumped energy increased from 600 to 400 nm, the signal build-up process (band filling process) will become slower.[40] As a result, the build-up time reduced from ∼4.9 to ∼2.8 ps when the pumped wavelengths converted from 400 to 600 nm.

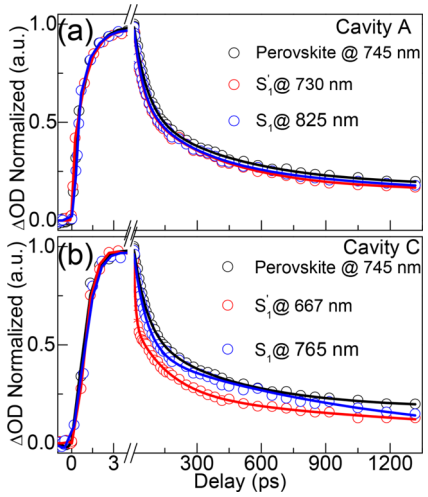

Figure 7. These dynamics curves pumped with 600 nm are split to two parts with the signal buildup representing band filling process and signal decay denoting relaxation process. The bare perovskite (black dots and lines) is as the reference. Representatively, (a) and (b), respectively, show the dynamics of S'_1 and S_1 created around band-edge level (∼745 nm) in cavities A and C.

Fluences-Dependent Relaxation Process. As mention above, we have observed that the charge carriers triggered in perovskite films show strong fluence-dependent characteristics as shown in Figure 3f.[38,39] It has been demonstrated that the perovskite charge carriers were indeed modulated by cavity resonance in perovskite-cavity complex MIM system. As a result, these created states should have both optical properties from cavity resonance and perovskite charge carriers. This is to say, the relaxation process of new states is not only faster but also should be fluences-dependent. Typically, we studied the fluence-dependent decay dynamics of S'_1 and S_1 created around band edge level in cavity A under 400 nm excitation. Figure 8a, b, and c, respectively, show the normalized relaxation kinetics traces of perovskite band edge transition, S_1, and S'_1 under a range of pump intensities from 11 to 112 μJ/cm^2. The dynamic spectrogram in Figure 8b and c show the strong fluences-dependent characteristics with faster relaxation rates for S_1 and S'_1. The quantitative analyzed data is shown in Figure 8d. As respect, it can be readily read that with the increasing pump

DOI: 10.1021/acs.jpcc.6b04072
J. Phys. Chem. C 2016, 120, 13295−13302

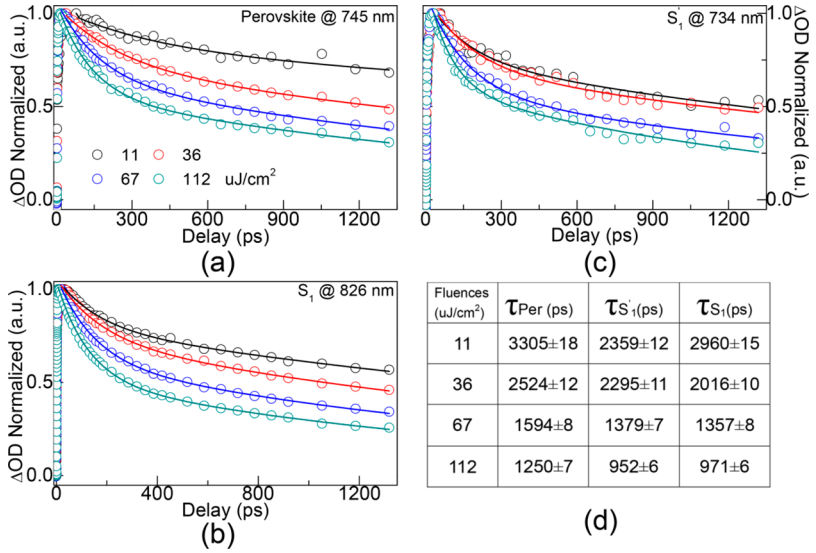

Fluences (uJ/cm^2)	τ_{Per} (ps)	$\tau_{S'_1}$(ps)	τ_{S_1}(ps)
11	3305±18	2359±12	2960±15
36	2524±12	2295±11	2016±10
67	1594±8	1379±7	1357±8
112	1250±7	952±6	971±6

Figure 8. Representatively, (a), (b), and (c), respectively, show the normalized relaxation dynamics curves of perovskite band edge, S_1, and S'_1 in cavity A pumped with 400 nm under a range of pump intensities between 11 and 112 μJ/cm^2. (d) Fitted lifetimes of band-edge relaxation processes of perovskite band edge, S_1 and S'_1. The new states relaxation process shows to be not only strongly fluences-dependent, but also faster compared with bare perovskite.

fluences, the lifetime of bare perovskite band edge level decreased from 3305 ± 18 to 1250 ± 7 ps, S'_1 decreased from 2359 ± 12 to 952 ± 6 ps, and S_1 decreased from 2960 ± 15 to 971 ± 6 ps. The data told us that the news states indeed is the outcome of interaction between cavity resonance and perovskite carriers in perovskite−cavity complex system.

CONCLUSIONS

In this paper, we have performed comprehensive study on the optical properties of organometal halide perovskite modulated by microcavities in perovskite−cavity complex system. Coupled states confirmed from reflective steady-state and time-resolved TA experiments clearly show the tunable coupling manipulation of cavity resonance on the characteristics of perovskite charges carriers. Given the broad absorption spectrum of perovskite $CH_3NH_3PbI_xCl_{3-x}$, the cavity resonant energy can be selectively designed to manipulate the photophysical characteristics of perovskite charge carriers at different levels. Through this work, it is found that (1) the binate new states created around cavity−matter resonance at different perovskite levels are mutual independent. (2) Band filling process of these created states is unchanged, while the relaxation process is accelerated by cavity. (3) These binate new states are half-cavity and half-carriers, so the resultant relaxation processes are also fluences-dependent. This interesting perovskite−cavity complex modulating system may lead to a series of optical applications in perovskite devices.

AUTHOR INFORMATION

Corresponding Authors

*E-mail: haiyu_wang@jlu.edu.cn. Tel.: +86 431 8516 8281.
*E-mail: hbsun@jlu.edu.cn. Tel.: +86 431 8516 8281.

Notes

The authors declare no competing financial interest.

ACKNOWLEDGMENTS

The authors would like to acknowledge National Natural Science Foundation of China (Grant Nos. 21473076 and 21473077), the 973 Project (Grants #2014CB921302 and 2011CB013003), Natural Science Foundation of China (NSFC Grant Nos. 21273096 and 61378053), and Doctoral Fund Ministry of Education of China (Grant 20130061110048).

REFERENCES

(1) Kavonkin, A.; Baumberg, J.; Malpuech, G.; Laussy, F. *Microcavities*; Springer: New York, 2007.
(2) Ameling, R.; Giessen, H. Cavity Plasmonics: Large Normal Mode Splitting of Electric and Magnetic Particle Plasmons Induced by a Photonic Microcavity. *Nano Lett.* **2010**, *10*, 4394−4398.
(3) Gomez, D. E.; Lo, S. S.; Davis, T. J.; Hartland, G. V. Picosecond Kinetics of Strongly Coupled Excitons and Surface Plasmon Polaritons. *J. Phys. Chem. B* **2013**, *117*, 4340−4346.
(4) Benz, A.; Campione, S.; Liu, S.; Montaño, I.; Klem, J. F.; Allerman, A.; Wendt, J. R.; Sinclair, M. B.; Capolino, F.; Brener, I. Strong coupling in the sub-wavelength limit using metamaterial nanocavities. *Nat. Commun.* **2013**, *4*, 2882−2889.
(5) Gomez, D. E.; Vernon, K. C.; Mulvaney, P.; Davis, T. J. Surface Plasmon Mediated Strong Exciton-Photon Coupling in Semiconductor Nanocrystals. *Nano Lett.* **2010**, *10*, 274−278.
(6) Coles, D. M.; Niccolo, S.; Paolo, M.; Caspar, C.; Lagoudakis, P. G.; Savvidis, P. G.; Lidzey, D. G. Polariton-mediated energy transfer between organic dyes in a strongly coupled optical microcavity. *Nat. Mater.* **2014**, *13*, 712−719.
(7) Lai, Y. Y.; Lan, Y. P.; Lu, T. C. Strong light−matter interaction in ZnO microcavities. *Light: Sci. Appl.* **2013**, *2*, e76.
(8) Jaynes, E. T.; Cummings, F. W. Comparison of quantum and semiclassical radiation theories with application to the beam maser. *Proc. IEEE* **1963**, *51*, 89−109.
(9) Roland, A.; Alexander, B.; Christian, D.; Jakob, R.; Christoph, B. Coupling of a single nitrogen-vacancy center in diamond to a fiber-based microcavity. *Phys. Rev. Lett.* **2013**, *110*, 243602.
(10) Putz, S.; Krimer, D.; Amsuess, R.; Valookaran, A.; Noebauer, T.; Schmiedmayer, J.; Rotter, S.; Majer, J. Protecting a spin ensemble against decoherence in the strong-coupling regime of cavity QED. *Nat. Phys.* **2014**, *10*, 720−724.
(11) Maunz, P.; Puppe, T.; Schuster, I.; Syassen, N.; Pinkse, P. W. H.; Rempe, G. Normal-mode spectroscopy of a single-bound-atom-cavity system. *Phys. Rev. Lett.* **2005**, *94*, 033002.
(12) Wu, Y.; Yang, X. Jaynes-cummings model for a trapped ion in any position of a standing wave. *Phys. Rev. Lett.* **1997**, *78*, 3086−3088.

DOI: 10.1021/acs.jpcc.6b04072
J. Phys. Chem. C 2016, 120, 13295−13302

(13) Thompson, R. J.; Rempe, G.; Kimble, H. J. Observation of normal-mode splitting for an atom in an optical cavity. *Phys. Rev. Lett.* **1992**, *68*, 1132−1135.
(14) Miller, R.; Northup, T. E.; Birnbaum, K. M.; Boca, A.; Boozer, A. D.; Kimble, H. J. Trapped atoms in cavity QED: coupling quantized light and matter. *J. Phys. B: At., Mol. Opt. Phys.* **2005**, *38*, S551−S565.
(15) Hakala, T. K.; Toppari, J. J.; Kuzyk, A.; Pettersson, M.; Tikkanen, H.; Kunttu, H.; Törma, P. Vacuum rabi splitting and strong-coupling dynamics for surface-plasmon polaritons and rhodamine 6G molecules. *Phys. Rev. Lett.* **2009**, *103*, 053602.
(16) Hayashi, S.; Ishigaki, Y.; Fujii, M. Plasmonic effects on strong exciton-photon coupling in metal-insulator-metal microcavities. *Phys. Rev. B: Condens. Matter Mater. Phys.* **2012**, *86*, 045408.
(17) Coles, D.; Adawi, A. M.; Clark, C.; Michetti, P.; Rajendran, S. K.; Brida, D.; Polli, D.; Cerullo, G.; Lidzey, D. G. Ultrafast polariton relaxation dynamics in an organic semiconductor microcavity. *Phys. Rev. B: Condens. Matter Mater. Phys.* **2011**, *83*, 245309.
(18) Agranovich, V. M.; Litinskaia, M.; Lidzey, D. G. Cavity polaritons in microcavities containing disordered organic semiconductors. *Phys. Rev. B: Condens. Matter Mater. Phys.* **2003**, *67*, 085311.
(19) Bellessa, J.; Bonnand, C.; Plenet, J. C.; Mugnier, J. Strong coupling between surface plasmons and excitons in an organic semiconductor. *Phys. Rev. Lett.* **2004**, *93*, 3.
(20) Schwartz, T.; Hutchison, J. A.; Genet, C.; Ebbesen, T. W. Reversible switching of ultrastrong light-molecule coupling. *Phys. Rev. Lett.* **2011**, *106*, 196405.
(21) Zhang, Z. Y.; Wang, H. Y.; Du, J. L.; Zhang, X. L.; Hao, Y. W.; Chen, Q. D.; Sun, H. B. Strong coupling in hybrid plasmon-modulated nanostructured cavities. *Appl. Phys. Lett.* **2014**, *105*, 191117.
(22) Zhang, B.; Wang, Z.; Brodbeck, S.; Schneider, C.; Kamp, M.; Höfling, S.; Deng, H. Zero dimensional polariton laser in a sub-wavelength grating based vertical microcavity. *Light: Sci. Appl.* **2014**, *3*, e135.
(23) Ding, K.; Ning, C. Z. Metallic subwavelength-cavity semiconductor nanolasers. *Light: Sci. Appl.* **2012**, *1*, e20.
(24) Christogiannis, N.; Somaschi, N.; Michetti, P.; Coles, D. M.; Savvidis, P. G.; Lagoudakis, P. G.; Lidzey, D. G. Characterizing the electroluminescence emission from a strongly coupled organic semiconductor microcavity LED. *Adv. Opt. Mater.* **2013**, *1*, 503−509.
(25) Mazzeo, M.; Genco, A.; Gambino, S.; Ballarini, D.; Mangione, F.; Stefano, O. D.; Patanè, S.; Savasta, S.; Sanvitto, D.; Gigli, G. Ultrastrong light-matter coupling in electrically doped microcavity organic light emitting diodes. *Appl. Phys. Lett.* **2014**, *104*, 233303.
(26) Kéna-Cohen, S.; DavancO, M.; Forrest, S. R. Strong exciton-photon coupling in an organic single crystal microcavity. *Phys. Rev. Lett.* **2008**, *101*, 116401.
(27) Kéna-Cohen, S.; Forrest, S. R. Room-temperature polariton lasing in an organic single-crystal microcavity. *Nat. Photonics* **2010**, *4*, 371−375.
(28) Wu, X. Q.; Xiao, Y.; Meng, C.; Zhang, X. N.; Yu, S. L.; Wang, Y. P.; Yang, C. X.; Guo, X.; Ning, C. Z.; Tong, L. M. Hybrid Photon-Plasmon Nanowire Lasers. *Nano Lett.* **2013**, *13*, 5654−5659.
(29) Tsotsis, P.; Eldridge, P. S.; Gao, T.; Tsintzos, S. I.; Hatzopoulos, Z.; Savvidis, P. G. Lasing threshold doubling at the crossover from strong to weak coupling regime in GaAs microcavity. *New J. Phys.* **2012**, *14*, 023060.
(30) Zhang, B.; Wang, Z.; Brodbeck, S.; Schneider, C.; Kamp, M.; Höfling, S.; Deng, H. Zero dimensional polariton laser in a sub-wavelength grating based vertical microcavity. *Light: Sci. Appl.* **2014**, *3*, e135.
(31) Cristofolini, P.; Christmann, G.; Tsintzos, S. I.; Deligeorgis, G.; Konstantinidis, G.; Hatzopoulos, Z.; Savvidis, P. G.; Baumberg, J. J. Coupling Quantum Tunneling with Cavity Photons. *Science* **2012**, *336*, 704−707.
(32) Salomon, A.; Genet, C.; Ebbesen, T. W. Molecule-light complex: dynamics of hybrid molecule-surface plasmon states. *Angew. Chem., Int. Ed.* **2009**, *48*, 8748−8751.
(33) Hao, Y. W.; Wang, H. Y.; Zhang, Z. Y.; Zhang, X. L.; Chen, Q. D.; Sun, H. B. Time-resolved fluorescence anisotropy of surface plasmon coupled emission on metallic gratings. *J. Phys. Chem. C* **2013**, *117*, 26734−26739.
(34) Juluri, B. K.; Lu, M.; Zheng, Y. B.; Huang, T. J.; Jensen, L. Coupling between molecular and plasmonic resonances: effect of molecular absorbance. *J. Phys. Chem. C* **2009**, *113*, 18499−18503.
(35) Zhang, Z. Y.; Wang, H. Y.; Du, J. L.; Zhang, X. L.; Hao, Y. W.; Chen, Q. D.; Sun, H. B. Surface plasmon-modulated fluorescence on 2D metallic silver gratings. *IEEE Photonics Technol. Lett.* **2015**, *27*, 821−823.
(36) Vasa, P.; Wang, W.; Pomraenke, R.; Lammers, M.; Maiuri, M.; Manzoni, C.; Cerullo, G.; Lienau, C. Real-time observation of ultrafast Rabi oscillations between excitons and plasmons in metal nanostructures with J-aggregates. *Nat. Photonics* **2013**, *7*, 128−132.
(37) Torma, P.; Barnes, W. L. Strong coupling between surface plasmon polaritons and emitters. *Rep. Prog. Phys.* **2015**, *78*, 013901.
(38) Manser, J. S.; Kamat, P. V. Band filling with free charge carriers in organometal halide perovskites. *Nat. Photonics* **2014**, *8*, 737−743.
(39) Zhang, Z. Y.; Chen, X.; Wang, H. Y.; Xv, M.; Gao, B. R.; Chen, Q. D.; Sun, H. B. Elucidating the band structure and free charge carrier dynamics of pure and impurities doped $CH_3NH_3PbI_{3-x}Cl_x$ perovskite thin films. *Phys. Chem. Chem. Phys.* **2015**, *17*, 30084−30089.
(40) Wu, X. X.; M Tuan, T.; Daniel, N.; Haiming, Z.; Zachariah, N.; Owen, J. S.; Yaffe, O.; Kudisch, B. J.; Zhu, X. Y. Trap states in lead iodide perovskites. *J. Am. Chem. Soc.* **2015**, *137*, 2089−2096.

DOI: 10.1021/acs.jpcc.6b04072
J. Phys. Chem. C 2016, 120, 13295−13302